

Hund interaction, spin-orbit coupling and the mechanism of superconductivity in strongly hole-doped iron pnictides

Oskar Vafek¹ and Andrey V. Chubukov²

¹*Department of Physics and National High Magnetic Field Laboratory,
Florida State University, Tallahassee, Florida 32306 USA*

²*School of Physics and Astronomy, University of Minnesota, Minneapolis, MN 55455, USA*
(Dated: November 14, 2018)

We present a novel mechanism of s -wave pairing in Fe-based superconductors. The mechanism involves holes near d_{xz}/d_{yz} pockets *only* and is applicable primarily to strongly hole doped materials. We argue that as long as the renormalized Hund's coupling J exceeds the renormalized inter-orbital Hubbard repulsion U' , any finite spin-orbit coupling gives rise to s -wave superconductivity. This holds even at weak coupling and regardless of the strength of the intra-orbital Hubbard repulsion U . The transition temperature grows as the hole density decreases. The pairing gaps are four-fold symmetric, but anisotropic, with the possibility of eight accidental nodes along the larger pocket. The resulting state is consistent with the experiments on KFe_2As_2 .

PACS numbers:

Introduction. The pairing mechanism in iron-based superconductors (FeSCs) remains the subject of intense debates [1]. A common scenario is that superconductivity (SC) is mediated by anti-ferromagnetic spin fluctuations, which are enhanced by the presence Fermi pockets of both hole and electron type [1–3]. This scenario yields an s -wave pairing amplitude with opposite sign on hole and electron pockets. Such an s^{+-} gap structure is consistent with experiments on moderately doped FeSCs which contain hole and electron pockets.

However, SC is also observed in strongly doped FeSCs with only hole or only electron pockets [4–12]. For these systems, it is not clear why spin fluctuations should be strong enough to overcome Coulomb repulsion.

In this paper we focus on the systems with only hole pockets, such as $\text{K}_x\text{Ba}_{1-x}\text{Fe}_2\text{As}_2$. For KFe_2As_2 , angle-resolve photoemission (ARPES) experiments show that only hole pockets are present [5, 6]. Yet, $T_c \approx 3\text{K}$ in KFe_2As_2 and increases as x decreases. The electronic structure of KFe_2As_2 consists of three hole pockets centered at Γ and hole “barrels” near $M = (\pi, \pi)$ in the Brillouin zone corresponding to a single Fe-As layer with two Fe atoms per primitive unit cell. The inner and the middle pockets at Γ have the symmetry of d_{xz} and d_{yz} orbitals, while the outer has the symmetry of the d_{xy} orbital [3].

There is no consensus at the moment among both experimentalists and theorists about the *pairing* symmetry in KFe_2As_2 . On the one hand, non-phase-sensitive measurements on KFe_2As_2 , such as thermal conductivity and Raman scattering, were interpreted as evidence for a d -wave gap [7–9]. On the other, laser ARPES reported full gap along the inner hole Fermi surface (FS), eight nodes along the middle FS, and negligible gap along the outer (d_{xy}) pocket [6]. This was interpreted as evidence of s -wave pairing [6, 13]. Specific heat data [10] on KFe_2As_2 were also interpreted in favor of s -wave with multiple gaps.

Existing theoretical proposals for superconductivity in

KFe_2As_2 explore the idea that the origin of the pairing in this system is the same as in FeSCs with hole and electron pockets, i.e., that the pairing is promoted by weak magnetic fluctuations. This mechanism has been analyzed within RPA [14, 15] and within the renormalization group (RG) [16], and was recently re-discovered [17]. The outcome is that, depending on parameters, spin fluctuations either favor s^{+-} SC with the gap changing sign between the inner and the middle d_{xz}/d_{yz} pockets [14, 15], or d -wave SC with the gap predominantly residing on the outer d_{xy} pocket [16].

Each scenario has a potential to explain superconductivity in KFe_2As_2 , but the key shortcoming of both is that s -wave and the d -wave attractions are very weak [15] because the mechanism is essentially of Kohn-Luttinger type [18]. Additionally, the d -wave pairing scenario yields the largest gap on the d_{xy} pocket, which is inconsistent with laser ARPES [6].

In this paper we propose a new mechanism for SC in KFe_2As_2 and other materials with only hole pockets. Consistent with laser ARPES[6], we assume that the pairing involves mainly holes from d_{xz}/d_{yz} pockets (see Fig.1), and neglect the hole barrels near (π, π) and the d_{xy} pocket at Γ where the observed pairing gap is much smaller. The pairing in our theory arises from the combination of two factors: sizable Hund's electron-electron interaction J and sizable spin-orbit (SO) interaction λ . Specifically, we argue that the system develops an s -wave SC as soon as J exceeds the inter-orbital Hubbard repulsion U' , *regardless* of the value of the intra-orbital Hubbard repulsion U . The effective dimensionless coupling constant in the s -wave pairing channel scales as $N_0(J - U') \left(\frac{\lambda}{\mu}\right)^2$, where N_0 is the density of states and μ is the chemical potential. That J is substantial has been discussed in the context of “Hund metal” [19, 20]. The magnitude of λ is also quite sizable in FeSCs. ARPES measurements (Ref.[21]) extracted $\lambda \sim 10 - 20\text{meV}$, comparable to μ .

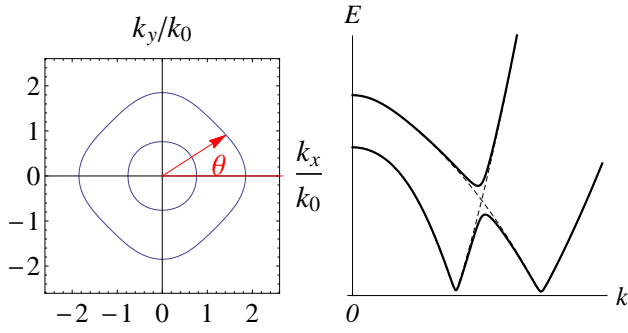


FIG. 1: Left panel: Illustrative Fermi surfaces (FS) for the d_{xz}/d_{yz} hole pockets, where $k_0 = \sqrt{2m\mu}$. In the SC state, the pairing amplitude on the outer Fermi surface is Δ_+ and on the inner Δ_- . Right panel: Schematic quasiparticle dispersion in the superconducting state (solid black lines). The gap away from the Fermi level is due to the A_{2g} pairing and is present already without SO. Once SO is included, the gaps on the FS appear. The dashed lines are approximations which capture the gaps on the FS only.

Without SO, the Cooper states at zero momentum can be classified according to their behavior separately under the crystal's point group operations and under spin $SU(2)$ rotations. As such, the on-site Hubbard-Hund interaction with positive U , U' , J and J' and $U > U'$, J, J' is repulsive in the s-wave (A_{1g}) and d-wave (B_{1g} and B_{2g}) spin singlet channels. The interaction in the A_{2g} spin-triplet channel, however, avoids U and is $\frac{1}{2}(U' - J)$. It is attractive when $J > U'$ [22]. By itself, an attraction in the A_{2g} channel does *not* necessarily lead to the Cooper instability because the pairing occurs between fermions from different bands and the pairing susceptibility is not logarithmically large at small temperature, T . Besides, A_{2g} pairing does not open gaps on the Fermi surfaces (see Fig.1). The situation changes when $\lambda \neq 0$ because SO coupling mixes the A_{1g} spin singlet and the A_{2g} spin triplet pairs [24]. The pairing susceptibility in A_{1g} channel diverges as $\log T$ at small T because the order parameter contains fermion pairs from the same band. We argue that s-wave superconductivity emerges as soon as $J > U'$. Remarkably, this conclusion is unaffected by the presence of a much stronger U despite the fact that the U determines the repulsion in the A_{1g} spin singlet channel.

The gaps on the two hole pockets are four-fold symmetric, but anisotropic. The solution of the self-consistency equations shows that the overall gap on the *larger* FS is smaller, in part, due to destructive interference between the A_{1g} and the A_{2g} components. For some range of parameters, the gap on this pocket has eight accidental nodes, as shown in the Fig.3. The relative magnitude of the A_{1g} and the A_{2g} components does not contain $\log T$, nevertheless, their ratio has a non-trivial temperature (T) dependence even at weak coupling. This may lead to a possibility that such accidental nodes appear only below some $T < T_c$.

Our results are summarized in Figs.2 and 3. We argue below that they are consistent with several experimental findings on $K_x\text{Ba}_{1-x}\text{Fe}_2\text{As}_2$ for $x \approx 1$.

The model. We consider the itinerant model with two Γ -centered hole pockets made out of d_{xz} and d_{yz} orbitals (see Fig. 1). The effective Hamiltonian $\mathcal{H} = H_0 + H_{int}$ for the low-energy states near Γ can be obtained, quite generally, using the method of invariants [24, 25], without the need to assume a particular microscopic model. The non-interacting part is

$$H_0 = \sum_{\mathbf{k}} \sum_{\alpha, \beta = \uparrow, \downarrow} \psi_{\mathbf{k}, \alpha}^\dagger (h_{\mathbf{k}} \delta_{\alpha\beta} + h^{SO} s_{\alpha\beta}^z) \psi_{\mathbf{k}, \beta}, \quad (1)$$

where the doublet $\psi_{\mathbf{k}, \sigma}^\dagger = \left(d_{Yz, \sigma}^\dagger(\mathbf{k}), -d_{Xz, \sigma}^\dagger(\mathbf{k}) \right)$, and

$$h_{\mathbf{k}} = \begin{pmatrix} \mu - \frac{\mathbf{k}^2}{2m} + bk_x k_y & c(k_x^2 - k_y^2) \\ c(k_x^2 - k_y^2) & \mu - \frac{\mathbf{k}^2}{2m} - bk_x k_y \end{pmatrix}, \quad (2)$$

$$h^{SO} = \lambda \begin{pmatrix} 0 & -i \\ i & 0 \end{pmatrix}. \quad (3)$$

The coefficients μ, m, b, c , and the SO coupling λ are material specific, but the forms of $h_{\mathbf{k}}$ and h^{SO} are universal.

The 4-fermion interaction Hamiltonian can also be written out in terms of the low energy doublet. Assuming spin $SU(2)$ symmetry and local interaction, we can express H_{int} in real space as

$$H_{int} = \sum_{j=0}^3 \frac{g_j}{2} \int d^2\mathbf{r} : \psi_{\sigma}^\dagger(\mathbf{r}) \tau_j \psi_{\sigma}(\mathbf{r}) \psi_{\sigma'}^\dagger(\mathbf{r}) \tau_j \psi_{\sigma'}(\mathbf{r}) : \quad (4)$$

where $::$ implies normal ordering, the repeated spin indices σ, σ' are summed over, $\tau_0 = \mathbb{1}$ and the three Pauli matrices τ_j act on the two components of the doublet. The four couplings g_j can be parameterized as $g_0 = \frac{1}{2}(U + U')$, $g_1 = \frac{1}{2}(J + J')$, $g_2 = \frac{1}{2}(J - J')$, and $g_3 = \frac{1}{2}(U - U')$. We emphasize that g_i 's include renormalizations from high energy modes and, in general, U, U', J , and J' are not the same as the *bare* Hubbard and Hund's interaction terms.

For $\lambda = 0$, the pairing can be decomposed into spin singlet A_{1g} , B_{1g} , and B_{2g} channels, as well as the spin triplet A_{2g} . The corresponding couplings are [24, 26] $g_{A_{1g}} = \tilde{g}_0 = (U + J')/2$, $g_{B_{1g}} = (U - J')/2$, $g_{B_{2g}} = (U' + J)/2$, and $g_{A_{2g}} = \tilde{g}_2 = \frac{1}{2}(g_0 - g_1 - g_2 - g_3) = (U' - J)/2$. The interactions in A_{1g} , B_{1g} , and B_{2g} channels are repulsive as the intra orbital Hubbard U is the largest local interaction. However the interaction in A_{2g} channel is attractive if $J > U'$. We assume this to hold. The A_{2g} order parameter is

$$\Delta_2 = \frac{1}{2} \tilde{g}_2 \langle \psi_{\alpha}^T(\mathbf{r}) \tau_2 (i s^z s^y)_{\alpha\beta} \psi_{\beta}(\mathbf{r}) \rangle. \quad (5)$$

Because τ_2 is antisymmetric and $i s^z s^y$ is symmetric, this order parameter is spin triplet. For $\lambda = 0$, Δ_2 in the

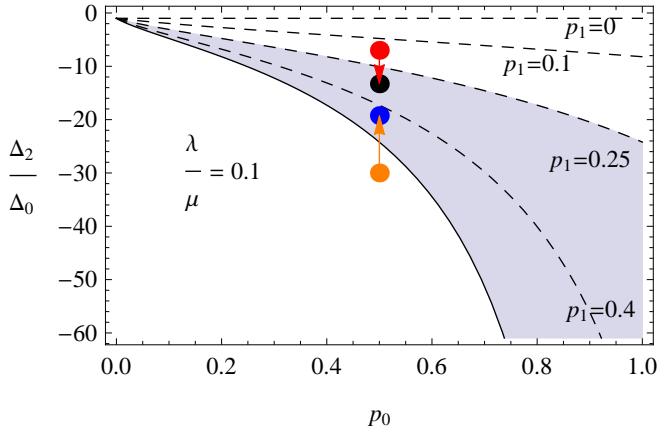


FIG. 2: The phase diagram at $T = 0$ calculated at a fixed ratio of the SO coupling λ to Fermi energy μ . Displayed are the boundaries of the nodal region, which depend on the ratio of A_{2g} (Δ_2) and A_{1g} (Δ_0) components of the pairing gap at $T = 0$. They also depend on p_0 and p_1 , dimensionless parameters which enter into the angle dependence of the normal state band dispersion as in Eqs.(9) and (10). The pairing amplitudes on the larger and the smaller Fermi surfaces are $\Delta_+ = \Delta_0 + (\lambda/|\vec{B}_{\mathbf{k}}|)\Delta_2$ and $\Delta_- = \Delta_0 - (\lambda/|\vec{B}_{\mathbf{k}}|)\Delta_2$, respectively; $2|\vec{B}_{\mathbf{k}}|$ is the energy of the band splitting (9). Shaded area marks the appearance of the accidental nodes in Δ_+ for $p_1 = 0.25$. For a different value of p_1 , the upper boundary of the shaded area shifts to the corresponding dashed line, while the lower boundary is p_1 -independent. Below (above) the shaded region, the signs of Δ_+ and Δ_- are opposite (same) and the pairing state can be viewed as s^{+-} (s^{++}). Interestingly, numerical solutions of the self-consistency equations find that it is possible to start outside of the nodal region at T_c (red and orange circles) and end up inside of it at $T = 0$ (black and blue circles).

band basis is composed entirely of fermions from different pockets. The susceptibility for such inter-pocket pairing does not contain the Cooper logarithm, and hence the attraction in A_{2g} channel alone does not give rise to Cooper pairing, at least at weak coupling. However, in the presence of the SO interaction, an arbitrarily weak A_{2g} attraction gives rise to a pairing instability, as we now show.

Role of SO coupling. For $\lambda \neq 0$, the A_{1g} and the A_{2g} channel in Eq.(5) mix[24]. Nevertheless, the A -channels and the B -channels remain decoupled. We focus on the A_{1g} channels because of the attraction in A_{2g} . Due to A_{2g}/A_{1g} mixing, the order parameter Δ_2 receives a contribution from fermions residing in the *same* band. The corresponding normal state pairing susceptibility is logarithmically large at small T . There is a caveat, however – the spin singlet A_{1g} pairing component is strongly repulsive. Our goal is to analyze whether it prevents pairing when $\tilde{g}_2 < 0$. To this end, we also introduce the conventional spin singlet A_{1g} order parameter,

$$\Delta_0 = \frac{1}{2}\tilde{g}_0\langle\psi_{\alpha}^T(\mathbf{r})\mathbb{1}(-is^y)_{\alpha\beta}\psi_{\beta}(\mathbf{r})\rangle, \quad (6)$$

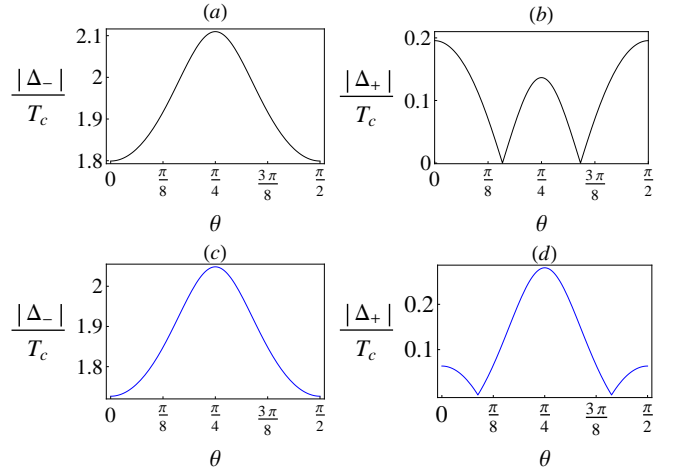


FIG. 3: Angle dependence of the gap at $T = 0$ on the inner (a) and the outer (b) hole Fermi surfaces (FS) for parameters corresponding to the (black) end point of the down (red) arrow in Fig.2. (c) and (d) show the same but for the parameters corresponding to the (blue) end point of the up (orange) arrow in Fig.2. In both cases, there are eight nodal points on the outer FS.

and obtain the set of two coupled equations for Δ_2 and Δ_0 (Ref. [27]). At T_c , we have for $\tilde{g}_2 < 0$ and $\tilde{g}_0 > 0$

$$\begin{aligned} -\frac{\Delta_0}{\tilde{g}_0} &= \sum_{\rho=\pm} \int \frac{d^2\mathbf{k}}{(2\pi)^2} \frac{\tanh \frac{\xi_{\rho}}{2T_c}}{2\xi_{\rho}} \left(\Delta_0 + \rho\Delta_2 \frac{\lambda}{|\vec{B}_{\mathbf{k}}|} \right), \quad (7) \\ -\frac{\Delta_2}{\tilde{g}_2} &= \sum_{\rho=\pm} \int \frac{d^2\mathbf{k}}{(2\pi)^2} \frac{1}{2\xi_{\rho}} \tanh \frac{\xi_{\rho}}{2T_c} \times \quad (8) \\ &\times \left(\Delta_2 \left(\frac{\lambda^2}{\vec{B}_{\mathbf{k}}^2} + \frac{\xi_{\rho}}{A_{\mathbf{k}}} \left(1 - \frac{\lambda^2}{\vec{B}_{\mathbf{k}}^2} \right) \right) + \rho\Delta_0 \frac{\lambda}{|\vec{B}_{\mathbf{k}}|} \right), \end{aligned}$$

where the normal state band dispersion has the form

$$\xi_{\pm} = A_{\mathbf{k}} \pm |\vec{B}_{\mathbf{k}}| = \mu - \frac{\mathbf{k}^2}{2m} \pm \sqrt{R_{\theta} \frac{\mathbf{k}^4}{4m^2} + \lambda^2}. \quad (9)$$

The angular anisotropy in momentum space enters via $0 < R_{\theta} < 1$, and is determined by the coefficients b and c in Eq.(35). We express it as

$$R_{\theta} = p_0 \left(\frac{1}{2} + p_1 + \left(\frac{1}{2} - p_1 \right) \cos 4\theta \right), \quad (10)$$

with $p_0 = 4m^2c^2$ and $p_1 = b^2/(8c^2)$. Without loss of generality, $0 < p_0 < 1$ and $0 < p_1 < \frac{1}{2}$. The Fermi surfaces shown in Fig.(1) correspond to $p_0 = 0.5$, $p_1 = 0.4$, and $\lambda/\mu = 0.1$. Eqs. (7-8) have the form

$$\begin{pmatrix} -\frac{1}{\tilde{g}_0} - \chi_{00}(T_c) & -\chi_{02}(T_c) \\ -\chi_{02}(T_c) & -\frac{1}{\tilde{g}_2} - \chi_{22}(T_c) \end{pmatrix} \begin{pmatrix} \Delta_0(T_c) \\ \Delta_2(T_c) \end{pmatrix} = 0. \quad (11)$$

Therefore, T_c is determined from requiring that the determinant vanishes

$$-\frac{1}{\tilde{g}_2} + \frac{\chi_{02}^2(T_c)}{\frac{1}{\tilde{g}_0} + \chi_{00}(T_c)} = \chi_{22}(T_c). \quad (12)$$

Brief inspection of (7-8) reveals that χ_{00} and χ_{22} scale as $\sim \ln \frac{1}{T}$. On the other hand, $\chi_{02}(T)$ remains finite due to an *exact cancellation* of two such logs. For $\mu \gg T_c$, we find

$$\chi_{02}(T_c) = \frac{m \lambda}{2\pi \mu} \int_0^{2\pi} \frac{d\theta}{2\pi} \frac{\tanh^{-1} \sqrt{R_\theta + (1 - R_\theta) \frac{\lambda^2}{\mu^2}}}{\sqrt{R_\theta + (1 - R_\theta) \frac{\lambda^2}{\mu^2}}}, \quad (13)$$

where $\tanh^{-1} x = \frac{1}{2} \ln \frac{1+x}{1-x}$. As a result, T_c is finite regardless of how weak is the attractive coupling, $\tilde{g}_2 < 0$, and how strong is the repulsive coupling $\tilde{g}_0 > 0$. Moreover, $\chi_{02}(T_c)\lambda/\mu$ is positive. From the gap equations we then find that $\Delta_0(T_c) = -\mathcal{C}\Delta_2(T_c)\lambda/\mu$, where $\mathcal{C} > 0$. The gaps on the two pockets are

$$\Delta_\pm = \Delta_0 \pm \frac{\lambda}{|\tilde{B}_k|} \Delta_2, \quad (14)$$

where Δ_+ is on the larger and Δ_- is on the smaller pocket. Analyzing the forms of these gaps, we find that (i) $|\Delta_+|$ is reduced relative to $|\Delta_-|$, (ii) the gaps are four-fold symmetric, but anisotropic, and (iii) for small $|\tilde{g}_2|$, Δ_0 is small compared to Δ_2 , forcing opposite signs of Δ_+ and Δ_- , i.e. s^{+-} gap structure.

Below T_c . The mean field equations below T_c are non-linear in $\Delta_0(T)$ and $\Delta_2(T)$. We eliminate the couplings \tilde{g}_0 and \tilde{g}_2 by expressing Δ_0 and Δ_2 in units of T_c . Solving the non-linear set we obtain $\Delta_{0,2}(T)/T_c$ and the ratio $K(T) = \Delta_0(T)/\Delta_2(T)$ in terms of the same ratio at T_c . In a general case, when the cross term $\chi_{0,2}$ is non-logarithmic, $K(T)$ remains the same as at T_c , at least at weak coupling. In our case, the situation is different because a finite $\chi_{02}(T)$ is due to subtle cancellation of the logs, and leftover terms are T -dependent. In the limit of $K(T_c) \ll 1$ we found analytically $K(T=0) = K(T_c)(1 + \mathcal{A})$, where $\mathcal{A} > 0$ (Ref. [27]). This also holds in the numerical solution of the mean-field equation, as indicated by the lower arrow in the Fig.2.

The numerical and analytical considerations show that the gap may have accidental nodes. The numerical solutions of the gap equations are shown in the Fig. 3. We see that, indeed, in some range of parameters, the gap on the larger hole pocket has eight accidental nodes. Interestingly, as shown in the Fig.2, we also found that over some range of parameters the nodes are absent at T_c , but appear at $T = 0$.

Comparison with experiments. Our results are consistent with several experimental findings on $\text{K}_x\text{Ba}_{1-x}\text{Fe}_2\text{As}_2$ for $x \approx 1$. Namely, (i) a larger gap on the inner hole pocket at Γ , with no nodes, (ii) a

smaller gap magnitude and the appearance of the accidental nodes on the larger d_{xz}/d_{yz} pocket (middle pocket at Γ), and (iii) angular correlation of the gap maxima on the two FSs are all consistent with the ARPES results [6]. The presence of the gap nodes is consistent with thermal conductivity and Raman scattering measurements [7–9], and the near-absence of the gap on the d_{xy} pocket is consistent with ARPES [6] and specific heat measurements [10]. We also analyzed the temperature dependence of the spin susceptibility $\chi(T)$ by adding a Zeeman coupling to \mathcal{H} . We found that $\chi(T)$ decreases below T_c for *any* orientation of the external magnetic field, even if Δ_0 is negligible compared to Δ_2 . This result is non-trivial because for $\lambda = 0$ the pairing was in A_{2g} spin-triplet channel, and $\chi(T)$ was *not* suppressed below T_c when the magnetic field is perpendicular to the triplet \mathbf{d} -vector. The decrease of $\chi(T)$ for any orientation of the magnetic field is consistent with the Knight shift measurements in KFe_2As_2 (Ref. [28]). Finally, from Eq.(8) we readily see that the prefactor of the Cooper logarithm in $\chi_{22}(T_c)$ contains a factor of λ^2/μ^2 . Therefore T_c *increases* as μ decreases, for fixed $\tilde{g}_{0,2}$ and fixed λ . When $T_c \ll \mu$, we found, to logarithmic accuracy,

$$\frac{T_c}{\mu} \sim \exp \left(-\sqrt{\left(1 + p_0 \frac{\mu^2}{\lambda^2}\right) \left(1 + 2p_0 p_1 \frac{\mu^2}{\lambda^2}\right)} \frac{\pi}{m|\tilde{g}_2|} \right) \quad (15)$$

The increase of T_c with decreasing x is consistent with the x dependence of T_c in $\text{K}_x\text{Ba}_{1-x}\text{Fe}_2\text{As}_2$ at $x \leq 1$. At smaller x , electron pockets appear, and s -wave pairing may become caused by interaction between fermions near hole and electron pockets.

Conclusions. In this paper we presented a novel mechanism of s -wave pairing in FeSC, which involves fermions near d_{xz}/d_{yz} hole pockets. When the renormalized Hund's interaction J exceeds the renormalized inter-orbital Hubbard repulsion U' , the interaction in A_{2g} channel is attractive. In the absence of SO coupling, this attraction would potentially give rise to spin-triplet superconductivity, but only when the attractive coupling exceeds a certain threshold. We argued that at a non-zero SO coupling, the same interaction gives an attraction in the s -wave channel, where the pairing condensate involves fermions from the same band and superconductivity emerges at an arbitrarily weak attraction. We demonstrated that T_c is only weakly affected by the large inter-orbital repulsion U in the A_{1g} channel, despite the fact that the SO coupling mixes the A_{2g} and the A_{1g} components. The gap functions are four-fold symmetric, but anisotropic, particularly on the larger FS, where over some range of parameters the gap has accidental nodes. Our results are consistent with ARPES and other experiments on strongly hole doped $\text{K}_x\text{Ba}_{1-x}\text{Fe}_2\text{As}_2$.

We thank E. Berg, P. Hirschfeld, R. Fernandes, M. Khodas, and J. Schmalian for useful discussions. OV was supported by NSF DMR-1506756. AVC was supported by the Office of Basic Energy Sciences, U.S. Department of Energy, under awards de-sc0014402. The

authors thank the Aspen Center for Physics, where part of this work was performed, for its hospitality. ACP is

supported by NSF grant PHY-1066293.

-
- [1] For recent reviews see J-P Paglione and R.L. Greene, *Nature Phys.* **6**, 645 (2010), I.I. Mazin, *Nature* **464**, 183 (2010), H.H. Wen and S. Li, *Annu. Rev. Condens. Matter Phys.*, **2**, 121 (2011), D.N. Basov and A.V. Chubukov, *Nature Physics* **7**, 241 (2011), P.J. Hirschfeld, M.M. Korshunov, and I.I. Mazin, *Rev. Prog. Phys.* **74**, 124508 (2011), A.V. Chubukov, *Annual Review of Condensed Matter Physics* **3**, 57 (2012); R. M. Fernandes, A. V. Chubukov, and J. Schmalian, *Nature Phys.* **10**, 97 (2014).
- [2] I. I. Mazin, D. J. Singh, M. D. Johannes, and M. H. Du, *Phys. Rev. Lett.* **101**, 057003 (2008); K. Kuroki, S. Onari, R. Arita, H. Usui, Y. Tanaka, H. Kontani, and H. Aoki *Phys. Rev. Lett.* **101**, 087004 (2008); A. V. Chubukov, D. Efremov, and I. Eremin, *Phys. Rev. B* **78**, 134512 (2008).
- [3] S. Graser, T. A. Maier, P. J. Hirschfeld, and D. J. Scalapino, *New J. Phys.* **11**, 025016 (2009).
- [4] T. Yoshida, I. Nishi, A. Fujimori, M. Yi, R. G. Moore, D. Lu, Z. Shen, K. Kihou, P. M. Shirage, H. Kito, C. H. Lee, A. Iyo, H. Eisaki, and H. Harima, arXiv:1007.2698; K. Hashimoto, A. Serafin, S. Tonegawa, R. Katsumata, R. Okazaki, T. Saito, H. Fukazawa, Y. Kohori, K. Kihou, C. H. Lee, A. Iyo, H. Eisaki, H. Ikeda, Y. Matsuda, A. Carrington, T. Shibauchi, *Phys. Rev. B* **82**, 014526 (2010); T. Terashima et al., *J. Phys. Soc. Jpn.* **79**, 053702 (2010).
- [5] T. Sato, K. Nakayama, Y. Sekiba, P. Richard, Y.-M. Xu et al., *Phys. Rev. Lett.* **103**, 047002 (2009); V. B. Zabolotnyy, D. V. Evtushinsky, A. A. Kordyuk, D. S. Inosov, A. Koitzsch, A. V. Boris, G. L. Sun, C. T. Lin, M. Knupfer, B. Buechner, A. Varykhalov, R. Follath, S. V. Borisenko, *Physica C* **469**, 448-451 (2009); D. V. Evtushinsky, T. K. Kim, A. A.Kordyuk, V. B. Zabolotnyy, B. Büchner, A. V. Boris, D. L. Sun, C. T. Lin, H. Q. Luo, Z. S.Wang, H. H. Wen, R. Follath, and S. V. Borisenko, arXiv:1106.4584. The electronic structure with 3 hole pockets at Γ and hole blades at the corners of the Brillouin zone (BZ) is consistent with DFT band structure calculations for this material [see e.g., T. Terashima, M. Kimata, N. Kurita, H. Satsukawa, A. Harada, K. Hazama, M. Imai, A. Sato, K. Kihou, C.-H. Lee, H. Kito, H. Eisaki, A. Iyo, T. Saito, H. Fukazawa, Y. Kohori, H. Harima, and S. Uji, *J. Phys. Soc. Jpn.* **79**, 053702 (2010)].
- [6] K. Okazaki, Y. Ota, Y. Kotani, W. Malaeb, Y. Ishida, T. Shimojima, T. Kiss, S. Watanabe, C.-T. Chen, K. Kihou, C. H. Lee, A. Iyo, H. Eisaki, T. Saito, H. Fukazawa, Y. Kohori, K. Hashimoto, T. Shibauchi, Y. Matsuda, H. Ikeda, H. Miyahara, R. Arita, A. Chainani, S. Shin, *Science* **337**, 1314 (2012); Y. Ota, K. Okazaki, Y. Kotani, T. Shimojima, W. Malaeb, S. Watanabe, C. -T. Chen, K. Kihou, C. H. Lee, A. Iyo, H. Eisaki, T. Saito, H. Fukazawa, Y. Kohori, and S. Shin, *Phys. Rev. B* **89**, 081103 (2014).
- [7] J. K. Dong, S. Y. Zhou, T. Y. Guan, H. Zhang, Y. F. Dai, X. Qiu, X. F. Wang, Y. He, X. H. Chen, and S. Y. Li, *Phys. Rev. Lett.* **104**, 087005 (2010); J.-Ph. Reid, M. A. Tanatar, A. Juneau-Fecteau, R. T. Gordon, S. Rene de Cotret, N. Doiron-Leyraud, T. Saito, H. Fukazawa, Y. Kohori, K. Kihou, C. H. Lee, A. Iyo, H. Eisaki, R. Prozorov, and L. Taillefer, *Phys. Rev. Lett.* **109**, 087001 (2012). For alternative explanation of thermal conductivity data see D. Watanabe, T. Yamashita, Y. Kawamoto, S. Kurata, Y. Mizukami, T. Ohta, S. Kasahara, M. Yamashita, T. Saito, H. Fukazawa, Y. Kohori, S. Ishida, K. Kihou, C. H. Lee, A. Iyo, H. Eisaki, A. B. Vorontsov, T. Shibauchi, and Y. Matsuda, *Phys. Rev. B* **89**, 115112 (2014).
- [8] For the behavior of T_c under pressure see F. F. Tafti, A. Juneau-Fecteau, M-E. Delage, S. Rene de Cotret, J-Ph. Reid, A. F. Wang, X-G. Luo, X. H. Chen, N. Doiron-Leyraud, and L. Taillefer, *Nature Phys.* **9**, 349 (2013) (for KFe_2As_2), and F. F. Tafti, J. P. Clancy, M. Lapointe-Major, C. Collignon, S. Faucher, J. Sears, A. Juneau-Fecteau, N. Doiron-Leyraud, A. F. Wang, X. G. Luo, X. H. Chen, S. Desgreniers, Young-June Kim, and Louis Taillefer, *Phys. Rev. B* **89**, 134502 (2014) (for CsFe_2As_2).
- [9] T. Böhm, A.F. Kemper, B. Moritz, F. Kretzschmar, B. Muschler, H.-M. Eiter, R. Hackl, T. P. Devereaux, D. J. Scalapino, and Hai-Hu Wen, *Phys. Rev. X* **4**, 041046 (2014). For an alternative explanation see M. Khodas, A. V. Chubukov, and G. Blumberg *Phys. Rev. B* **89**, 245134 (2014).
- [10] F. Hardy *et al.* *Phys. Soc. Jpn.* **83**, 014711 (2014)
- [11] J. Guo, S. Jin, G. Wang, S. Wang, K. Zhu, T. Zhou, M. He, and X. Chen, *Phys. Rev. B* **82**, 180520(R) (2010). See Y. Liu, Z. C. Li, W. P. Liu, G. Friemel, D. S. Inosov, R. E. Dinnebier, Z. J. Li, and C. T. Lin, *Supercond. Sci. Technol.* **25**, 075001 (2012); T. Qian, X.-P. Wang, W.-C. Jin, P. Zhang, P. Richard, G. Xu, X. Dai, Z. Fang, J.-G. Guo, X.-L. Chen, H. Ding, *Phys. Rev. Lett.* **106**, 187001 (2011).
- [12] G. Friemel et al, *Phys. Rev. B* **85**, 140511 (2012).
- [13] More recent theoretical studies [29, 30] pointed out that a full gap at the FS wavevectors does not necessarily rule out d -wave because the gap minimum does not reside along the normal state FS. Yet, for KFe_2As_2 the measured angle variation of the gap on the inner pocket is still much weaker than the one expected for a d -wave gap [30].
- [14] K. Suzuki, H. Usui, and K. Kuroki, *Phys. Rev. B* **84**,144514 (2011); S. Maiti, M.M. Korshunov, T.A. Maier, P.J. Hirschfeld, A.V. Chubukov, *Phys. Rev. Lett.* **107**, 147002 (2011); *Phys. Rev. B* **84**, 224505 (2011); C. Platt, G. Li, M. Fink, W. Hanke, and R. Thomale, arXiv:1607.00412.
- [15] S. Maiti, M. M. Korshunov, A. V. Chubukov, *Phys. Rev. B* **85**, 014511 (2012).
- [16] R. Thomale, C. Platt, W. Hanke, J. Hu, and B. A. Bernevig, *Phys. Rev. Lett.* **107**, 117001 (2011).
- [17] T. Ong, P. Coleman, and J. Schmalian, *PNAS* **113**, 5486 (2016).
- [18] see e.g. S. Maiti and A.V. Chubukov, “Superconductivity from a repulsive interaction” in “Novel Superconductivity from a repulsive interaction”

tors”, Chapter 15, Bennemann and Ketterson eds., Oxford Press 2014 and references therein

- [19] K. Haule, and G. Kotliar, New. J. Phys. **11** 025021 (2009); J. Hu, Phys. Rev. X **3**, 031004 (2013); A. Georges, L. de Medici, and J. Mravlje, Annu. Rev. Condens. Matter Phys. **4**, 137-178 (2013).
- [20] L. Fanfarillo, G. Giovannetti, M. Capone, and E. Bascones, arXiv: 1608.06672 and references therein.
- [21] S. V. Borisenko, D. V. Evtushinsky, Z.-H. Liu, I. Morozov, R. Kappenberger, S. Wurmehl, B. Büchner, A. N. Yaresko, T. K. Kim, M. Hoesch, T. Wolf, and N. D. Zhigadlo Nature Physics **12**, 311 (2016)
- [22] A pairing due to positive $J - U'$ has been proposed earlier in Ref.[23]. That proposal, however, is for the nodal p -wave spin-triplet pairing on electron pockets. Such a pairing is *entirely absent* on the hole pockets. NMR measurement on KFe_2As_2 found a suppression of Knight shift for all directions of the magnetic field and thus ruled out a pure spin-triplet superconductivity for this material.
- [23] P.A. Lee and X.-G. Wen Phys. Rev. B **78**, 144517 (2008).
- [24] V. Cvetkovic and O. Vafek, Phys. Rev. B **88**, 134510 (2013).
- [25] R. M. Fernandes and O. Vafek, Phys. Rev. B **90**, 214514 (2014).
- [26] A. V. Chubukov, M. Khodas, and R. M. Fernandes, arXiv:1602.05503.
- [27] See Supplementary Material for details.
- [28] H. Fukazawa, T. Saito, Y. Yamada, K. Kondo, M. Hirano, Y. Kohori, K. Kuga, A. Sakai, Y. Matsumoto, S. Nakatsuji, K. Kihou, A. Iyo, C. H. Lee and H. Eisaki, J. of the Phys. Soc. of Japan, **80**, SA118 (2011).
- [29] E. M. Nica, R. Yu, and Q. Si, arXiv:1505.04170.
- [30] A.V. Chubukov, R. Fernandes, and O. Vafek, PRB, to appear.

I. SUPPLEMENTARY MATERIAL

A. Pairing in the orbital and band representations

In this Section we discuss how one can understand the results of random-phase approximation (RPA) and func-

tional renormalization group (fRG) analysis of the pairing in systems with only hole pockets. Spin fluctuations generally require the presence of both hole and electron pockets and are weak in systems with only one type of pockets. Yet, both RPA and fRG calculations showed that even a weak renormalization of Hubbard and Hund interactions gives rise to an attraction in s -wave and d -wave channels. The attractive interaction is weak and the corresponding T_c is truly small and is very likely much smaller than s -wave T_c that we obtained in this paper. Nevertheless, as a matter of principle, the attraction does appear in numerical calculations, and below we show how one can understand analytically why it emerges. Another goal of our discussion is to clarify the interplay between s -wave and d -wave order parameters in the orbital and the band basis.

We begin by noticing that in a system with a local Hubbard and Hund interaction, it is natural to classify the pairing states in the orbital basis because pairing interaction in this basis decouples between different channels. For the same model as in the bulk of the paper (i.e., the model of fermions on d_{xz} and d_{yz} orbitals near the Γ point), the order parameters in the s -wave (A_{1g}) and d -wave (B_{1g}) channels are

$$\begin{aligned}\Delta_{A_{1g}}^{orb} &= d_{xz,\uparrow}^\dagger d_{xz,\downarrow}^\dagger + d_{yz,\uparrow}^\dagger d_{yz,\downarrow}^\dagger, \\ \Delta_{B_{1g}}^{orb} &= d_{xz,\uparrow}^\dagger d_{xz,\downarrow}^\dagger - d_{yz,\uparrow}^\dagger d_{yz,\downarrow}^\dagger.\end{aligned}\quad (16)$$

The Hubbard-Hund local Hamiltonian contains intra-pocket and inter-pockets Hubbard terms (U and U' terms, respectively), the Hund exchange J term and the Hund pair hopping term J' . Out of these four terms, Hubbard U and Hund J' terms contribute to the pairing Hamiltonian at the mean-field level (i.e., without renormalizations). In momentum space, the pairing Hamiltonian takes the form

$$\begin{aligned}H_{orb} = & U \sum_{k,p} \left(d_{xz,k,\uparrow}^\dagger d_{xz,-k,\downarrow}^\dagger d_{xz,p,\downarrow} d_{xz,-p,\uparrow} + d_{yz,k,\uparrow}^\dagger d_{yz,-k,\downarrow}^\dagger d_{yz,p,\downarrow} d_{yz,-p,\uparrow} + h.c \right) \\ & + J' \sum_{k,p} \left(d_{xz,k,\uparrow}^\dagger d_{xz,-k,\downarrow}^\dagger d_{yz,p,\downarrow} d_{yz,-p,\uparrow} + d_{yz,k,\uparrow}^\dagger d_{yz,-k,\downarrow}^\dagger d_{xz,p,\downarrow} d_{xz,-p,\uparrow} + h.c \right)\end{aligned}\quad (17)$$

This Hamiltonian can be equivalently re-written as

$$H_{orb} = \frac{U + J'}{2} |\Delta_{A_{1g}}^{orb}| + \frac{U - J'}{2} |\Delta_{B_{1g}}^{orb}| \quad (18)$$

The corresponding eigenvalues $(U + J')/2$ for A_{1g} and $(U - J')/2$ for B_{1g} are both negative as long as $U > J'$. The corrections from dressing the interaction by particle-

hole bubbles cannot change the sign of the interaction, at least at weak coupling and away from a collective instability.

We now switch gears and consider s -wave and d -wave (A_{1g} and B_{1g}) order parameters in the band basis. For simplicity, we assume that hole pockets are circular. An extension to non-circular, but still C_4 -symmetric pock-

ets is straightforward and just complicates the formulas without changing the results.

Let's denote band fermions as d_1 and d_2 . A simple experimentation shows that there are four possible order parameters

$$\begin{aligned}\Delta_{s^{++}}^b(k) &= d_{1,k,\uparrow}^\dagger d_{1,-k,\downarrow}^\dagger + d_{2,k,\uparrow}^\dagger d_{2,-k,\downarrow}^\dagger \\ \Delta_{s^{+-}}^b(k) &= d_{1,k,\uparrow}^\dagger d_{1,-k}^\dagger - d_{2,k,\uparrow}^\dagger d_{2,-k,\downarrow}^\dagger \\ \Delta_{d^{++}}^b(k) &= \left(d_{1,k,\uparrow}^\dagger d_{1,-k}^\dagger + d_{2,k,\uparrow}^\dagger d_{2,-k,\downarrow}^\dagger \right) \cos 2\theta_k \\ \Delta_{d^{+-}}^b(k) &= \left(d_{1,k,\uparrow}^\dagger d_{1,-k}^\dagger - d_{2,k,\uparrow}^\dagger d_{2,-k,\downarrow}^\dagger \right) \cos 2\theta_k(19)\end{aligned}$$

where θ is the angle along each of the Fermi surfaces, counted from, say, x -axis. The first two order parameters have s -wave symmetry – a conventional s^{++} and

s^{+-} , which changes sign between the two bands. The other two have d -wave symmetry, again with or without additional sign change between the two pockets (d^{+-} and d^{++} , respectively).

Clearly, there are more options in the band basis than in the orbital basis. To understand why there is a (potential) discrepancy, we convert the local interaction from the orbital to the band basis. For circular pockets, the transformation from orbital to band basis is just a rotation:

$$\begin{aligned}d_{xz}(k, \sigma) &= d_1(k, \sigma) \cos \theta + d_2(k, \sigma) \sin \theta, \\ d_{yz}(k, \sigma) &= d_2(k, \sigma) \cos \theta - d_1(k, \sigma) \sin \theta; \quad (20)\end{aligned}$$

Transforming the interaction Hamiltonian, Eq. (17) from orbital to band basis, we obtain

$$\begin{aligned}H_b &= \sum_{k,p} \left(\frac{U+J'}{2} + \frac{U-J'}{2} \cos \theta_k \cos \theta_p \right) \left(d_{1,k,\uparrow}^\dagger d_{1,-k,\downarrow}^\dagger d_{1,p,\downarrow} d_{1,-p,\uparrow} + d_{2,k,\uparrow}^\dagger d_{2,-k,\downarrow}^\dagger d_{2,p,\downarrow} d_{2,-p,\uparrow} + h.c \right) \\ &+ \sum_{k,p} \left(\frac{U+J'}{2} - \frac{U-J'}{2} \cos \theta_k \cos \theta_p \right) \left(d_{1,k,\uparrow}^\dagger d_{1,-k,\downarrow}^\dagger d_{2,p,\downarrow} d_{2,-p,\uparrow} + d_{2,k,\uparrow}^\dagger d_{2,-k,\downarrow}^\dagger d_{1,p,\downarrow} d_{1,-p,\uparrow} + h.c \right) \quad (21)\end{aligned}$$

This Hamiltonian can be equivalently re-written as

$$H_b = \frac{U+J'}{2} \sum_k |\Delta_{s^{++}}^b(k)|^2 + \frac{U-J'}{2} \sum_k |\Delta_{d^{+-}}^b(k)|^2 \quad (22)$$

which is the same as Eq. (18). We see that, as expected, only two gap functions are present, one in A_{1g} channel and the other in B_{1g} channel. The two other order parameters, s^{+-} and d^{++} , do not appear in the Hamiltonian, i.e., the corresponding couplings are strictly zero.

Let's now continue with the band basis analysis and include the effect of renormalization of the pairing inter-

action by particle-hole bubbles. This can be second-order renormalization by a single bubble (Kohn-Luttinger effect) or it may include RPA series of particle-hole bubbles. In the latter case the effect of RPA summation can be re-expressed as due to collective spin fluctuations. Spin fluctuations are rather weak in KFe_2As_2 , so most likely the dominant renormalization at not too strong coupling comes from a single particle-hole bubble. The renormalization affects differently the prefactors in different terms in Eq. (21). In a generic case, H_b changes to

$$\begin{aligned}H_b &= \\ &\sum_{k,p} (U_{11} + \bar{U}_{11} \cos \theta_k \cos \theta_p) \left(d_{1,k,\uparrow}^\dagger d_{1,-k,\downarrow}^\dagger d_{1,p,\downarrow} d_{1,-p,\uparrow} + h.c \right) + (U_{22} + \bar{U}_{22} \cos \theta_k \cos \theta_p) \left(d_{2,k,\uparrow}^\dagger d_{2,-k,\downarrow}^\dagger d_{2,p,\downarrow} d_{2,-p,\uparrow} + h.c \right) \\ &+ \sum_{k,p} (U_{12} - \bar{U}_{12} \cos \theta_k \cos \theta_p) \left(d_{1,k,\uparrow}^\dagger d_{1,-k,\downarrow}^\dagger d_{2,p,\downarrow} d_{2,-p,\uparrow} + d_{2,k,\uparrow}^\dagger d_{2,-k,\downarrow}^\dagger d_{1,p,\downarrow} d_{1,-p,\uparrow} + h.c \right) \quad (23)\end{aligned}$$

where in the absence of renormalizations $U_{11} = U_{22} = U_{12} = (U+J')/2$ and $\bar{U}_{11} = \bar{U}_{22} = \bar{U}_{12} = (U-J')/2$. To make presentation easier to follow, we assume that $U_{11} = U_{22}$ and $\bar{U}_{11} = \bar{U}_{22}$ even after renormalization,

but keep $U_{11} \neq U_{12}$ and $\bar{U}_{11} \neq \bar{U}_{12}$. Decomposing H_b into contributions with different order parameters, like we did in going from (21) to (22) we immediately find that H_b now contains contributions with all four order

parameters from (19):

$$\begin{aligned}
H_b = & \frac{U_{11} + U_{12}}{2} \sum_k |\Delta_{s^{++}}^b(k)|^2 + \frac{U_{11} - U_{12}}{2} \sum_k |\Delta_{s^{+-}}^b(k)|^2 \\
& + \frac{\bar{U}_{11} + \bar{U}_{12}}{2} \sum_k |\Delta_{d^{+-}}^b(k)|^2 + \frac{\bar{U}_{11} - \bar{U}_{12}}{2} \sum_k |\Delta_{d^{++}}^b(k)|^2
\end{aligned} \tag{24}$$

For A_{1g} channel this is nothing but a well-known generation of s^{+-} interaction by a renormalization which makes intra-pocket repulsion different from inter-pocket repulsion. When renormalization makes U_{12} larger than U_{11} , the system develops an attractive interaction in s^{+-} channel, and arbitrary weak attraction already gives rise to a BCS instability in s^{+-} channel, despite strong repulsion in s^{++} channel (the situation becomes more complex beyond BCS as s^{++} and s^{+-} order parameters obviously belong to the same A_{1g} representation and hence in general do not decouple). The weak attraction in s^{+-} channel has been found in Ref. [15] using spin-fluctuation calculations and band structure for KFe_2As_2 and cited there as a potential reason for s^{+-} pairing in this material. Note, however, that the same mechanism may give rise to a weak d-wave (d^{++}) pairing, if renormalized \bar{U}_{12} exceeds \bar{U}_{11} .

We now go back to orbital basis and check how the interaction and the gap structure in s^{+-} and d^{++} channels looks like there. The gap structure is easily obtained by inverting the transformation (20):

$$\begin{aligned}
d_1(k, \sigma) &= d_{xz}(k, \sigma) \cos \theta - d_{yz}(k, \sigma) \sin \theta, \\
d_2(k, \sigma) &= d_{yz}(k, \sigma) \cos \theta + d_{xz}(k, \sigma) \sin \theta.
\end{aligned} \tag{25}$$

Substituting this transformation into (19) we indeed recover Eq. (16) for s^{++} and d^{+-} order parameters (labeled A_{1g} and B_{1g} in (16), modulo an additional $(1 + \cos 4\theta)$ factor in $\Delta_{B_{1g}}^{orb}$). The other two order parameters in the orbital representation are

$$\begin{aligned}
\Delta_{s^{+-}}^{orb} &= \left(d_{xz, \uparrow}^\dagger d_{xz, \downarrow}^\dagger - d_{yz, \uparrow}^\dagger d_{yz, \downarrow}^\dagger \right) \cos 2\theta, \\
\Delta_{d^{++}}^{orb} &= \left(d_{xz, \uparrow}^\dagger d_{xz, \downarrow}^\dagger + d_{yz, \uparrow}^\dagger d_{yz, \downarrow}^\dagger \right) \cos 2\theta
\end{aligned} \tag{26}$$

We see that s^{+-} order parameter in orbital representation is a product of B_{1g} order parameter from (16) and d -wave form factor $\cos 2\theta$. The product is indeed C_4 symmetric, as s -wave order parameter should be.

To see how these new order parameter emerge if we solve for the pairing in the orbital basis, without moving back and forth orbital basis, we re-express the renormalized interaction H_b in the orbital basis. Substituting (25) into (24) we find that the renormalization brings in additional pairing terms to originally local Hubbard-Hund interaction, in the form

$$\begin{aligned}
\delta H_{orb} = & \lambda_1 \sum_{k,p} \cos 2\theta_k \cos 2\theta_p \left(d_{xz, k, \uparrow}^\dagger d_{xz, -k, \downarrow}^\dagger d_{xz, p, \downarrow} d_{xz, -p, \uparrow} + d_{yz, k, \uparrow}^\dagger d_{yz, -k, \downarrow}^\dagger d_{yz, p, \downarrow} d_{yz, -p, \uparrow} + h.c \right) \\
& + \lambda_2 \sum_{k,p} \cos 2\theta_k \cos 2\theta_p \left(d_{xz, k, \uparrow}^\dagger d_{xz, -k, \downarrow}^\dagger d_{yz, p, \downarrow} d_{yz, -p, \uparrow} + d_{yz, k, \uparrow}^\dagger d_{yz, -k, \downarrow}^\dagger d_{xz, p, \downarrow} d_{xz, -p, \uparrow} + h.c \right)
\end{aligned} \tag{27}$$

where

$$\begin{aligned}
\lambda_1 &= \frac{U_{11} - U_{12}}{2} + \frac{\bar{U}_{11} - \bar{U}_{12}}{2}, \\
\lambda_2 &= -\frac{U_{11} - U_{12}}{2} + \frac{\bar{U}_{11} - \bar{U}_{12}}{2},
\end{aligned} \tag{28}$$

We see that additional terms in H_{orb} make the interaction in the orbital basis non-local and also dependent on the

direction in the momentum space. The interaction term δH_{orb} looks like a d -wave term because of $\cos 2\theta_k \cos 2\theta_p$ factors. However, $(U_{11} - U_{12})/2$ terms in λ_1 and λ_2 are also of different sign, and this additional sign change makes the corresponding part of δH_{orb} C_4 symmetric. Solving for the pairing right in the orbital basis we indeed obtain that C_4 -symmetric part of δH_{orb} gives rise to s^{+-} pairing in $U_{12} > U_{11}$, while C_4 anti-symmetric

part of δH_{orb} gives rise to d^{++} pairing in $\tilde{U}_{12} > \tilde{U}_{11}$.

B. Gap equations

The effective BCS Hamiltonian for coupled spin singlet A_{1g} and spin triplet A_{2g} order parameters is

$$\mathcal{H} \approx \mathcal{H}_{BdG} - L^2 \left(\frac{|\Delta_0|^2}{\tilde{g}_0} + \frac{|\Delta_2|^2}{\tilde{g}_2} \right), \quad (29)$$

where L^2 is the area of the system and

$$\mathcal{H}_{BdG} = \sum_{\mathbf{k}} \Psi_{\mathbf{k}}^\dagger H_{BdG}(\mathbf{k}) \Psi_{\mathbf{k}}, \quad (30)$$

where in the Nambu notation $\Psi_{\mathbf{k}}^\dagger = (\psi_{\mathbf{k}\uparrow}^\dagger, \psi_{-\mathbf{k}\downarrow}^T)$ and

$$H_{BdG}(\mathbf{k}) = \begin{pmatrix} h_{\mathbf{k}} + \lambda\tau_2 & \mathbb{1}\Delta_0 + \tau_2\Delta_2 \\ \mathbb{1}\Delta_0^* + \tau_2\Delta_2^* & -h_{\mathbf{k}} - \lambda\tau_2 \end{pmatrix}. \quad (31)$$

We used the fact that $h_{\mathbf{k}} = h_{-\mathbf{k}}^T$.

The linearized mean-field self-consistency equations at $T = T_c$ are presented in the main text. The equations below T_c are ($k_B = 1$)

$$-\frac{\Delta_0}{\tilde{g}_0} = \sum_{p=\pm} \int \frac{d^2\mathbf{k}}{(2\pi)^2} \frac{\tanh \frac{E_p}{2T}}{2E_p} \left(\Delta_0 + 4\Delta_2 \frac{A_{\mathbf{k}}\lambda + \Delta_0\Delta_2}{E_p^2 - E_{-p}^2} \right),$$

$$-\frac{\Delta_2}{\tilde{g}_2} = \sum_{p=\pm} \int \frac{d^2\mathbf{k}}{(2\pi)^2} \frac{\tanh \frac{E_p}{2T}}{2E_p} \times \left(\Delta_2 + 4\Delta_0 \frac{\vec{B}_{\mathbf{k}}^2 - \lambda^2}{E_p^2 - E_{-p}^2} + 4\Delta_0 \frac{A_{\mathbf{k}}\lambda + \Delta_0\Delta_2}{E_p^2 - E_{-p}^2} \right).$$

The coefficients $A_{\mathbf{k}}$ and $\vec{B}_{\mathbf{k}}$ are related to the parameters of the non-interacting Hamiltonian

$$H_0 = \sum_{\mathbf{k}} \sum_{\alpha,\beta=\uparrow,\downarrow} \psi_{\mathbf{k},\alpha}^\dagger (h_{\mathbf{k}}\delta_{\alpha\beta} + h^{SO} s_{\alpha\beta}^z) \psi_{\mathbf{k},\beta}, \quad (34)$$

where $\psi_{\mathbf{k},\sigma}^\dagger = (d_{Yz,\sigma}^\dagger(\mathbf{k}), -d_{Xz,\sigma}^\dagger(\mathbf{k}))$, and

$$h_{\mathbf{k}} = \begin{pmatrix} \mu - \frac{\mathbf{k}^2}{2m} + bk_x k_y & c(k_x^2 - k_y^2) \\ c(k_x^2 - k_y^2) & \mu - \frac{\mathbf{k}^2}{2m} - bk_x k_y \end{pmatrix}, \quad (35)$$

$$h^{SO} = \lambda \begin{pmatrix} 0 & -i \\ i & 0 \end{pmatrix}. \quad (36)$$

The relation are

$$h_{\mathbf{k}} + \lambda\tau_2 = A_{\mathbf{k}}\mathbb{1} + \vec{B}_{\mathbf{k}} \cdot \vec{\tau}. \quad (37)$$

The two branches of the Bogoliubov quasiparticle dispersion are

$$(32) E_{\pm} = \left(A_{\mathbf{k}}^2 + \vec{B}_{\mathbf{k}}^2 + \Delta_0^2 + \Delta_2^2 \pm 2\sqrt{A_{\mathbf{k}}^2 \vec{B}_{\mathbf{k}}^2 + \Delta_0^2 \Delta_2^2 + 2\Delta_0 \Delta_2 A_{\mathbf{k}} \lambda + \Delta_2^2 (\vec{B}_{\mathbf{k}}^2 - \lambda^2)} \right)^{\frac{1}{2}}. \quad (38)$$

We show it schematically by the bold lines in the right panel of Fig. 1 in the main text.

To understand $H_{BdG}(\mathbf{k})$ in the band basis, we perform (33) a unitary operation which diagonalizes $h_{\mathbf{k}} + \lambda\tau_2$. We find

$$\mathcal{U}^\dagger H_{BdG}(\mathbf{k}) \mathcal{U} = \begin{pmatrix} \xi_+ & 0 & \Delta_0 + \frac{\lambda}{|\vec{B}_{\mathbf{k}}|} \Delta_2 & -i\Delta_2 \sqrt{1 - \frac{\lambda^2}{\vec{B}_{\mathbf{k}}^2}} \\ 0 & \xi_- & i\Delta_2 \sqrt{1 - \frac{\lambda^2}{\vec{B}_{\mathbf{k}}^2}} & \Delta_0 - \frac{\lambda}{|\vec{B}_{\mathbf{k}}|} \Delta_2 \\ \Delta_0 + \frac{\lambda}{|\vec{B}_{\mathbf{k}}|} \Delta_2 & -i\Delta_2 \sqrt{1 - \frac{\lambda^2}{\vec{B}_{\mathbf{k}}^2}} & -\xi_+ & 0 \\ i\Delta_2 \sqrt{1 - \frac{\lambda^2}{\vec{B}_{\mathbf{k}}^2}} & \Delta_0 - \frac{\lambda}{|\vec{B}_{\mathbf{k}}|} \Delta_2 & 0 & -\xi_- \end{pmatrix}. \quad (39)$$

At low energy, we can ignore the off-diagonal terms in the pairing blocks. The Bogoliubov quasiparticle dispersion can be readily read off and approximated very well by

$$E_{\pm} \approx \sqrt{\xi_{\pm}^2 + \left(\Delta_0 \pm \frac{\lambda}{|\vec{B}_{\mathbf{k}}|} \Delta_2 \right)^2}, \quad (40)$$

where the band dispersion has the form

$$\xi_{\pm} = A_{\mathbf{k}} \pm |\vec{B}_{\mathbf{k}}| = \mu - \frac{\mathbf{k}^2}{2m} \pm \sqrt{R_{\theta} \frac{\mathbf{k}^4}{4m^2} + \lambda^2}. \quad (41)$$

As mentioned in the main text, we parameterize R_{θ} as

$$R_{\theta} = p_0 \left(\frac{1}{2} + p_1 + \left(\frac{1}{2} - p_1 \right) \cos 4\theta \right), \quad (42)$$

where, without loss of generality, $0 < p_0 < 1$ and $0 < p_1 < \frac{1}{2}$.

The top (bottom) sign in (41) corresponds to the outer (inner) Fermi surface. Eq.(40) corresponds to the dashed line in the right panel of Fig.1 of main text, which as we see, captures well the low energy avoided level crossing caused by pairing. It misses the level crossing at high energy, but at weak coupling this is unimportant. The form of the Eq.(39) makes it clear that for $\Delta_0 \rightarrow 0$, the pairing is of s_{\pm} nature. Moreover, it is anisotropic, because the zeros of ξ_{\pm} do not coincide with the minima of $|\vec{B}_{\mathbf{k}}|$. In addition, the gap is smaller on the outer Fermi surface, because the factor $|\vec{B}_{\mathbf{k}}|$ is larger there.

At weak coupling, when $T_c \ll \mu$ even if $\lambda/\mu = O(1)$, $|\Delta_0| \ll |\frac{\lambda}{|\vec{B}_{\mathbf{k}}|} \Delta_2|$. In this situation, one can approximate the gaps Δ_{\pm} by $\pm \frac{\lambda}{|\vec{B}_{\mathbf{k}}|} \Delta_2$. The values of Δ_+ and Δ_- are universally expressed via T_c . The expressions are particularly simple for $p_1 = 1/2$, when $R_{\theta} = p_0$ reduces to a constant. In this case we have

$$\left| \frac{\Delta_-}{\Delta_+} \right| = \frac{\sqrt{p_0 + (1 - p_0) \frac{\lambda^2}{\mu^2} + p_0}}{\sqrt{p_0 + (1 - p_0) \frac{\lambda^2}{\mu^2} - p_0}}, \quad (43)$$

$$|\Delta_+|^{\frac{|\Delta_-|}{|\Delta_-|+|\Delta_+|}} |\Delta_-|^{\frac{|\Delta_+|}{|\Delta_-|+|\Delta_+|}} = \Delta_{BCS}, \quad (44)$$

where $\Delta_{BCS} = 1.76T_c$.

C. The gap ratio

We now keep Δ_0 in the gap equation and compute the ratio $K(T) = \Delta_0(T)/\Delta_2(T)$. At weak coupling, when

$\Delta_2 \ll \mu$, the calculation of the gap ratio at $T = T_c$ yields $K(T_c) \ll 1$. In this limit, we found analytically

$$K(T = 0) \approx K(T_c)(1 + \mathcal{A}), \quad (45)$$

where

$$\mathcal{A} = \left(1 + \frac{\delta\chi_{02}}{\chi_{02}(T_c)} + \dots \right). \quad (46)$$

In (46)

$$\chi_{02}(T_c) = \frac{m \lambda}{2\pi \mu} \int_0^{2\pi} \frac{d\theta}{2\pi} \frac{\tanh^{-1} \sqrt{R_{\theta} + (1 - R_{\theta}) \frac{\lambda^2}{\mu^2}}}{\sqrt{R_{\theta} + (1 - R_{\theta}) \frac{\lambda^2}{\mu^2}}}, \quad (47)$$

and

$$\delta\chi_{02} = \frac{m \lambda}{2\pi \mu} \int_0^{2\pi} \frac{d\theta}{2\pi} \frac{\ln \frac{1 + \mathcal{F}(\theta, \frac{\lambda}{\mu})}{1 - \mathcal{F}(\theta, \frac{\lambda}{\mu})}}{\sqrt{R_{\theta} + (1 - R_{\theta}) \frac{\lambda^2}{\mu^2}}}, \quad (48)$$

where $\mathcal{F}(\theta, \frac{\lambda}{\mu}) = R_{\theta} / \sqrt{R_{\theta} + (1 - R_{\theta}) \frac{\lambda^2}{\mu^2}} < 1$. Because $\delta\chi_{02}$ and $\chi_{02}(T_c)$ have the same sign (the same as the sign of λ), their ratio is positive, hence $\mathcal{A} > 0$, i.e., the magnitude of Δ_0/Δ_2 is larger at $T = 0$ than at T_c .

For circular pockets, when $p_1 = 1/2$ and $R_{\theta} = p_0$, and for $\lambda \ll \mu$, we obtained a very simple result: $\mathcal{A} = 2$, i.e., the ratio Δ_0/Δ_2 at $T = 0$ is three times larger than at T_c .